

## Supporting Information

### Designing $\pi$ -Conjugated Polymer Blends with Improved Thermoelectric Power Factors

Ashkan Abtahi,<sup>a,b</sup> Stephen Johnson,<sup>c</sup> So Min Park,<sup>a,d</sup> Xuyi Luo,<sup>e</sup> Zhiming Liang,<sup>a</sup> Jianguo Mei,<sup>e</sup> and Kenneth R. Graham<sup>a,\*</sup>

<sup>a</sup>Department of Chemistry, University of Kentucky, Lexington, Kentucky 40506, United States

<sup>b</sup>Department of Physics, University of Kentucky, Lexington, Kentucky 40506, United States

<sup>c</sup>Department of Physics, Transylvania University, Lexington, Kentucky 40508, United States

<sup>d</sup>Department of Chemical and Materials Engineering, University of Kentucky, Lexington, Kentucky 40506, United States

<sup>e</sup>Department of Chemistry, Purdue University, West Lafayette, Indiana 47907, United States

#### I. Experimental Details

*Materials:* Mo(tfd)<sub>3</sub> was synthesized and supplied by the Marder group at the Georgia Institute of Technology according to a previously reported procedure.<sup>1</sup> The synthesis of PDPP-4T and PDPP-T-TT-T was performed by the Mei group at Purdue University and also followed previous references.<sup>2,3</sup> RR-P3HT and RRa-P3HT were purchased from Rieke metals. Bismuth was purchased from Kurt J. Lesker with 99.99% purity. Gold coins with 99.99% purity were thermally evaporated to form electric contacts. Anhydrous degassed chloroform (DriSolv, Ethanol stabilized, 99.8%) was used as a solvent.

*Sample preparation for Seebeck and electrical conductivity characterization:* Doped polymer solutions were prepared with a total polymer concentration of 5 mg/mL and a total dopant concentration of 1.16 mg/mL under a nitrogen environment in a glovebox (typically <0.1 ppm H<sub>2</sub>O and O<sub>2</sub>). Chloroform was degassed prior to use to remove oxygen using three freeze-pump-thaw cycles. Polymer solutions were stirred over night at 400-500 rpm at 35 °C. The dopant was then added to reach a doping concentration of 5 mole % dopant relative to the repeat unit of P3HT. Based on a polymer density of ca. 1.2 g/cm<sup>3</sup> and the density of Mo(tfd)<sub>3</sub> as 2.26 g/cm<sup>3</sup>, this doping

concentration is equal to ca. 10% by volume for all polymers. This concentration by volume was the same for all solutions to ensure the number of dopants in the solution per unit of volume is kept constant. The mixed solution of polymer and dopant was stirred at 400-500 rpm at 35 °C for an hour. To make the polymer blend solutions, stock solutions of the doped polymers were combined to make solutions with the desired polymer ratios. The polymer ratios are all given as weight ratios. 10×20 mm<sup>2</sup> glass slides were cleaned with sonication in aqueous detergent (sodium dodecyl sulfate, Sigma-Aldrich), deionized water, acetone, and 2-propanol each for 15 min. After drying them with nitrogen, they were exposed to UV-ozone treatment for 10 minutes to remove any remaining organic contamination. The clean substrates were transferred to the nitrogen filled glovebox and films were spun cast at 1000 rpm for 30 seconds with 3 seconds ramp time. For the films used for Seebeck measurements, a Q-tip wet with degassed chloroform was used to clean the doped polymer from regions where electrodes and bismuth were deposited. The film used for electrical conductivity were used as spun cast. Bismuth (100 nm, as temperature reference) and gold (50 nm, as electrodes) were thermally evaporated under vacuum with a shadow mask. The Seebeck coefficient was measured with a custom built setup.<sup>4</sup> The details of the Seebeck measurement geometry and system can be found in our previous publication.<sup>4</sup> The voltage across the polymer film and Bismuth film was measured by two Keithley 2100 multimeters and the temperature of the hot block was resistively heated and controlled with a TC200 Thorlab temperature controller. Sheet resistance was measured with a four-point probe setup consisting of Signatone S302-4 and Keithley 2450 source meter. To calculate electrical conductivity, film thickness was measured with a Dektak D6M/32 profilometer ( $\sigma = \frac{1}{R_{\square}t}$ ,  $\sigma$  is electrical conductivity,  $R_{\square}$  is sheet resistance and  $t$  is thickness of film).

*UV-vis absorbance:* UV-vis absorbance spectra were measured with an Ocean Optics QE Pro high-performance spectrometer with the sample inside of an integrating sphere.

*UPS:* Thin films for UPS were spun cast on non-patterned ITO-coated glass substrates (15 Ω/sq) with the same conditions as the films fabricated for electrical conductivity measurements. The samples were transferred to the UPS analysis chamber without air exposure. UPS measurements were taken with an Excitech H Lyman-α photon source (10.2 eV) coupled with a PHI 5600 ultrahigh vacuum system (pressure lower than  $1 \times 10^{-9}$  mbar during measurement) with a hemispherical electron energy analyzer, as detailed in our previous publication.<sup>5</sup>

*PDS sample preparation:* RR-P3HT and RRa-P3HT solutions were prepared with 20 mg/mL polymer concentrations and PDPP-4T and PDPP-T-TT-T were prepared with 10 mg/mL polymer concentration in degassed

chloroform. The solutions were stirred at 450 rpm and 35 °C overnight. The solutions were spun cast on cleaned quartz substrates at 800 rpms for 30 seconds in the nitrogen filled glovebox. The samples were sealed in moisture resistant packaging in the glovebox and transferred to Dr. Stephen Johnson at Transylvania University for PDS measurements.

## II. Arkhipov-Bässler model<sup>6</sup>

The average number of available hopping sites for a charge carrier starting at energy  $E_i$  whose hopping parameter is smaller than  $R$  is equal to:

$$n(E_i, R) = 4\pi \int_0^{R\frac{\alpha}{2}} r^2 dr \int_{-\infty}^{E_i + K_B T (R - r\frac{\alpha}{2})} g_u(E_j, E_F) dE_j = 4\pi \left[ \int_0^{R\frac{\alpha}{2}} r^2 dr \int_{-\infty}^{E_i} g_u(E_j, E_F) dE_j + \int_0^{R\frac{\alpha}{2}} r^2 dr \int_{E_i}^{E_i + K_B T (R - r\frac{\alpha}{2})} g_u(E_j, E_F) dE_j \right] \quad (\text{S.1})$$

The first term can be integrated separately and the second term can be simplified by changing the order of integration:

$$\begin{aligned} n(E_i, R) &= 4\pi \left[ \frac{1}{3} \left( R \frac{\alpha}{2} \right)^3 \int_{-\infty}^{E_i} g_u(E_j, E_F) dE_j + \int_{E_i}^{E_i + K_B T (R)} g_u(E_j, E_F) dE_j \int_0^{\frac{\alpha}{2} \left( R - \frac{E_j - E_i}{K_B T} \right)} r^2 dr \right] \\ &= 4\pi \left[ \frac{1}{3} \left( R \frac{\alpha}{2} \right)^3 \int_{-\infty}^{E_i} g_u(E_j, E_F) dE_j + \int_{E_i}^{E_i + K_B T (R)} g_u(E_j, E_F) dE_j \frac{1}{3} \left( R - \frac{E_j - E_i}{K_B T} \right)^3 \right] \\ &= \frac{4\pi}{3} \left( R \frac{\alpha}{2} \right)^3 \left[ \int_{-\infty}^{E_i} g_u(E_j, E_F) dE_j + \int_{E_i}^{E_i + K_B T (R)} \left( 1 - \frac{E_j - E_i}{R K_B T} \right)^3 g_u(E_j, E_F) dE_j \right] \quad (\text{S.2}) \end{aligned}$$

Further simplification will lead to equation 4. The probability density of hopping with hopping parameter  $R$  is shown by Poisson distribution as below:

$$P(E_i, R) = \frac{\partial n(E_i, R)}{\partial R} e^{-n(E_i, R)} \quad (\text{S.3})$$

So, the average hopping parameter is equal to:

$$\langle R \rangle (E_i) = \int_0^\infty R P(E_i, R) dR = \int_0^\infty R \frac{\partial n(E_i, R)}{\partial R} e^{-n(E_i, R)} dR \quad (\text{S.4})$$

Using integration by parts we arrive at:

$$\langle R \rangle (E_i) = -R e^{-n(E_i, R)} \Big|_0^\infty - \int_0^\infty (-e^{-n(E_i, R)}) dR = \int_0^\infty e^{-n(E_i, R)} dR \quad (\text{S.5})$$

First term is zero at both limits ( $\lim_{R \rightarrow \infty} n(E_i, R) = \infty$ ), so average  $R$  is simply equal to:

$$\langle R \rangle (E_i) = \int_0^\infty e^{-n(E_i, R)} dR \quad (\text{S.6})$$

Average squared jump distance is equal to:

$$\langle r^2 \rangle(E_i) = \frac{4\pi \int_0^{(R)(E_i)\frac{\alpha}{2}} \langle r^2 \rangle r^2 dr \int_{-\infty}^{E_i + K_B T \langle (R)(E_i) - r \frac{2}{\alpha} \rangle} g_u(E_j, E_F) dE_j}{4\pi \int_0^{(R)(E_i)\frac{\alpha}{2}} r^2 dr \int_{-\infty}^{E_i + K_B T \langle (R)(E_i) - r \frac{2}{\alpha} \rangle} g_u(E_j, E_F) dE_j} \quad (\text{S.7})$$

Using the same methods as in equations S.1 and S.2,  $\langle r^2 \rangle(E)$  is simplified to:

$$\langle r^2 \rangle(E_i) = \frac{3}{20} \langle (R)(E_i) \rangle^2 \alpha^2 \frac{\int_{-\infty}^{E_i} g_u(E_j, E_F) dE_j + \int_{E_i}^{E_i + K_B T \langle (R)(E_i) \rangle} g_u(E_j, E_F) \left(1 - \frac{E_j - E_i}{K_B T \langle (R)(E_i) \rangle}\right)^5 dE_j}{\int_{-\infty}^{E_i} g_u(E_j, E_F) dE_j + \int_{E_i}^{E_i + K_B T \langle (R)(E_i) \rangle} g_u(E_j, E_F) \left(1 - \frac{E_j - E_i}{K_B T \langle (R)(E_i) \rangle}\right)^3 dE_j} \quad (\text{S.8})$$

### III. Effect of $\frac{a}{\alpha}$ on TE properties

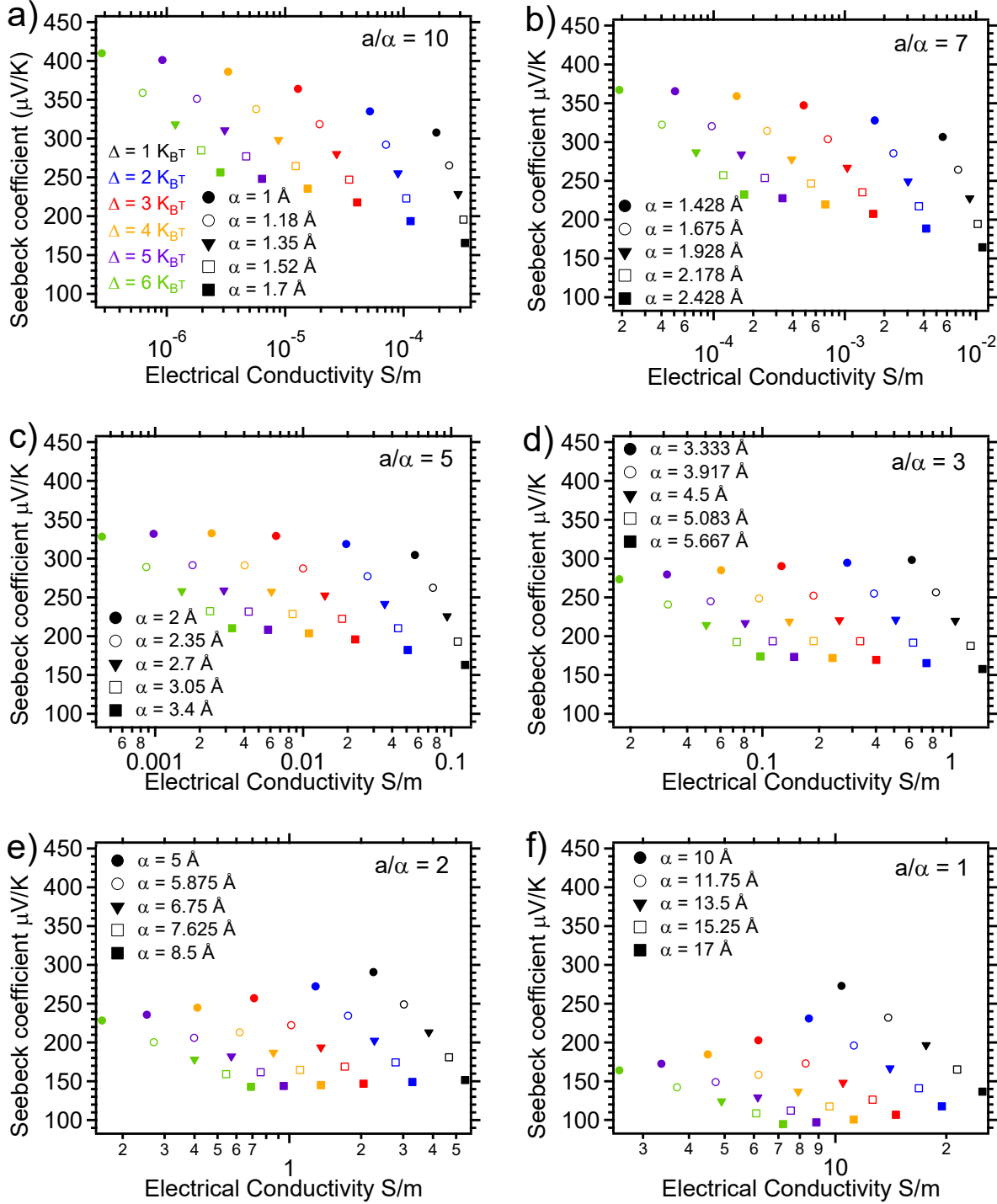


**Figure S1.** Seebeck coefficient vs. electrical conductivity. Parameters are  $N_c = 3 \times 10^{19} \text{cm}^{-3}$ ,  $v_0 = 10^{12} \text{s}^{-1}$ ,  $a$  has values of 1, 1.18, 1.35, 1.52 and 1.7 nm (corresponding to  $N_t = 10, 6.09, 4.06, 2.85$  and  $2.06 \times 10^{20} \text{cm}^{-3}$ ), and  $\Delta$  has values of ranging from 1 to  $6 K_B T$ .  $\alpha$  is chosen such that the ratio between  $a$  and  $\alpha$  is constant for each figure,  $\frac{a}{\alpha}$  is 10 for (a), 7 for (b), 5 for (c), 3 for (d), 2 for (e) and 1 for (f).

As explained in the main text, higher localization lengths for the same DOS width lead to higher electrical conductivity, while a narrower DOS width for the same localization length will also lead to higher electrical conductivity. As Figure S1 shows, as the electrical conductivities increase the effect of both localization length and DOS width on the Seebeck coefficient and electrical conductivity become smaller. For ratios of  $\frac{a}{\alpha}$  larger than 3, trends in the Seebeck coefficient are as explained in the main text, i.e., higher disorder and smaller localization lengths will result in higher Seebeck coefficients. By going to ratios of  $\frac{a}{\alpha}$  smaller than 3, the Seebeck coefficient will increase as the DOS width decreases and the localization length decreases. The reason for this is that at high charge carrier concentration in a broader DOS there are more charge carriers located at energies below the Fermi energy. In the situation where the localization length is small compared to the intrinsic length (which defines the total number of states), the charge carriers in the low energy states are partially trapped and cannot contribute to the transport, but if the localization length is large enough, in theory, they can contribute to the transport. In this case, these low energy charge carriers decrease the Seebeck coefficient. To maintain consistency with previous work<sup>7</sup> and prevent changes in trends due to the  $\frac{a}{\alpha}$  ratio, we maintain  $\frac{a}{\alpha} > 3$  in all calculations presented in the paper. Additionally, the trends in the Seebeck coefficient for  $\frac{a}{\alpha} > 3$  are consistent with trends found with Monte Carlo simulations, where the Seebeck coefficient increases with increasing energetic disorder.<sup>8</sup> Figure S2 highlights how the  $\frac{a}{\alpha}$  ratio influences the power factor.

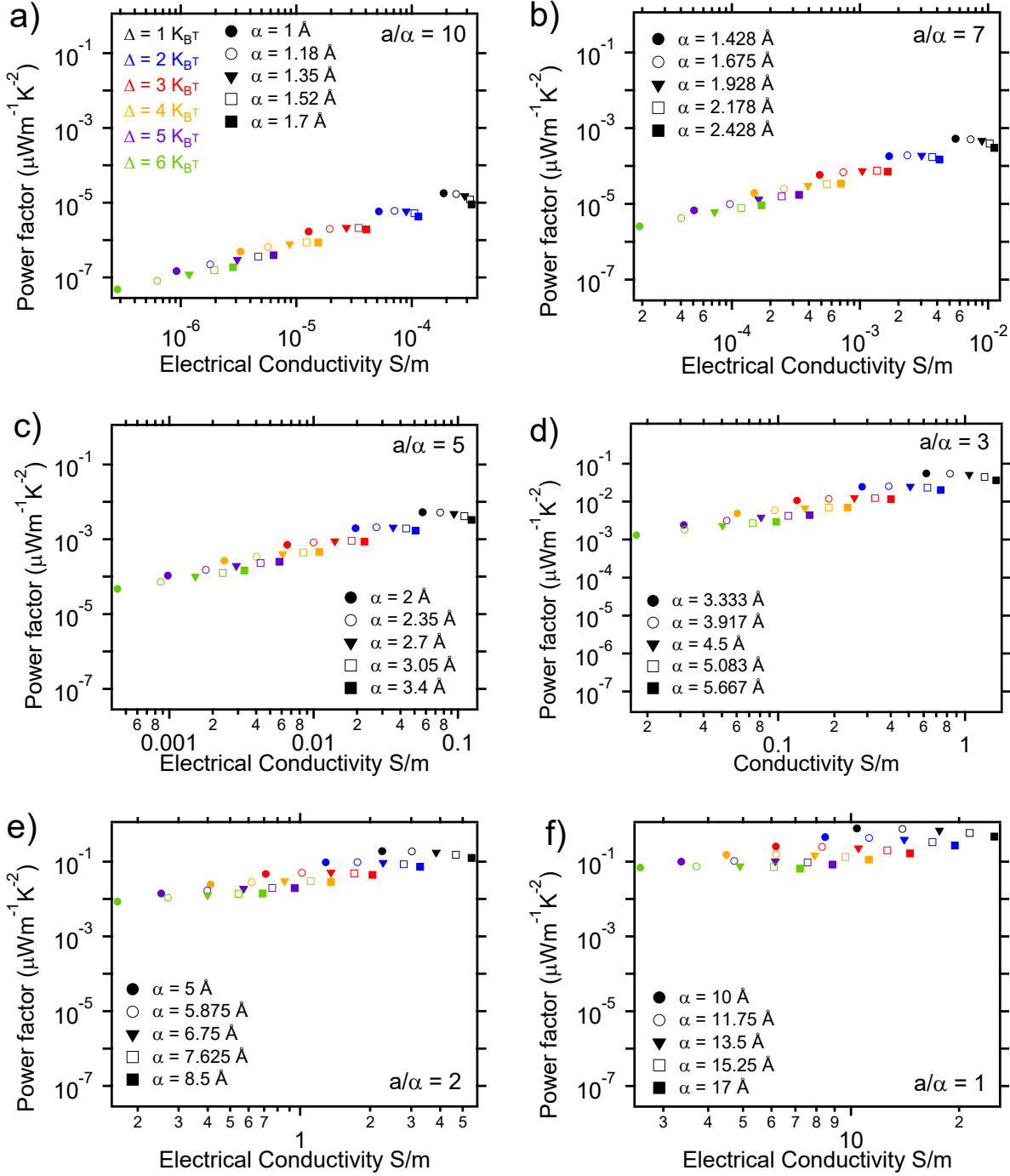


**Figure S2.** Power factor vs. electrical conductivity. Parameters are  $N_c = 3 \times 10^{19} \text{cm}^{-3}$ ,  $v_0 = 10^{12} \text{s}^{-1}$ ,  $a$  has values of 1, 1.18, 1.35, 1.52 and 1.7 nm (corresponding to  $N_t = 10, 6.09, 4.06, 2.85$  and  $2.06 \times 10^{20} \text{cm}^{-3}$ ),  $\Delta$  has values of 1-6  $K_B T$ .  $\alpha$  is chosen in such way that the ratio between  $a$  and  $\alpha$  is constant for each figure,  $\frac{a}{\alpha}$  is 10 for (a), 7 for (b), 5 for (c), 3 for (d), 2 for (e) and 1 for (f).

As we mentioned above, for  $\frac{a}{\alpha} > 3$  the trends in the power factor are the same as we explained in the main text. However, when  $\frac{a}{\alpha} < 3$ , as the DOS narrows the power factor still increases, but as the localization length increases the power factor decreases for a constant DOS width within all DOS widths examined.

#### IV. Fermi Energy in Polymer blends

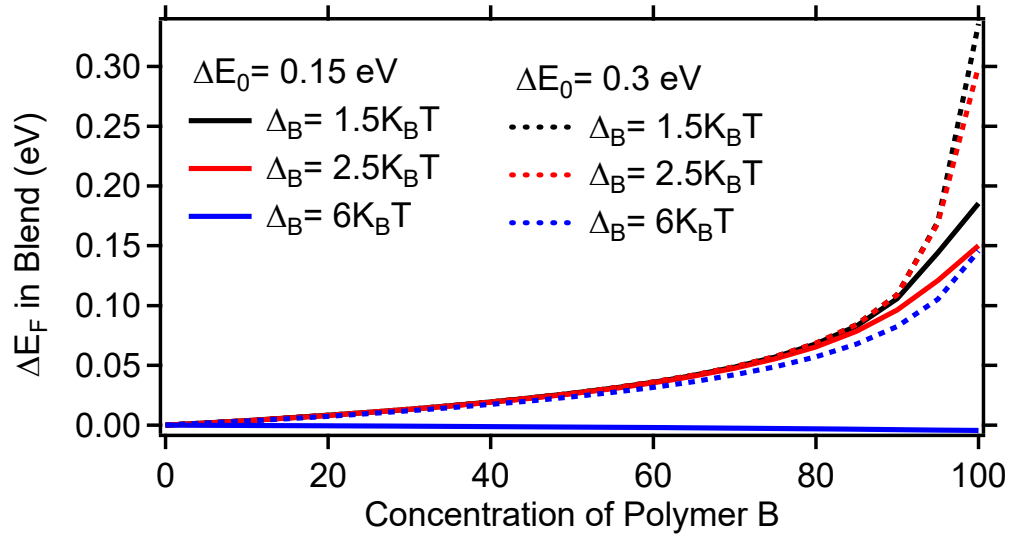


**Figure S3.** Fermi energy as a function of polymer concentration for added polymer with the same, narrower and broader DOS width at 0.15 and 0.3 eV offset. The Fermi energy of pure polymer A is set to be zero. Fitting parameters are  $N_{t,A}=N_{t,B}= 1 \times 10^{21} \text{ cm}^{-3}$ ,  $\Delta_A=2.5 K_B T$ ,  $\Delta_B=1.5, 2.5$  and  $6 K_B T$ ,  $\Delta E_0=0.15$  and  $0.3 \text{ eV}$ ,  $T=300 \text{ K}$  and  $N_C=3 \times 10^{19} \text{ cm}^{-3}$ .

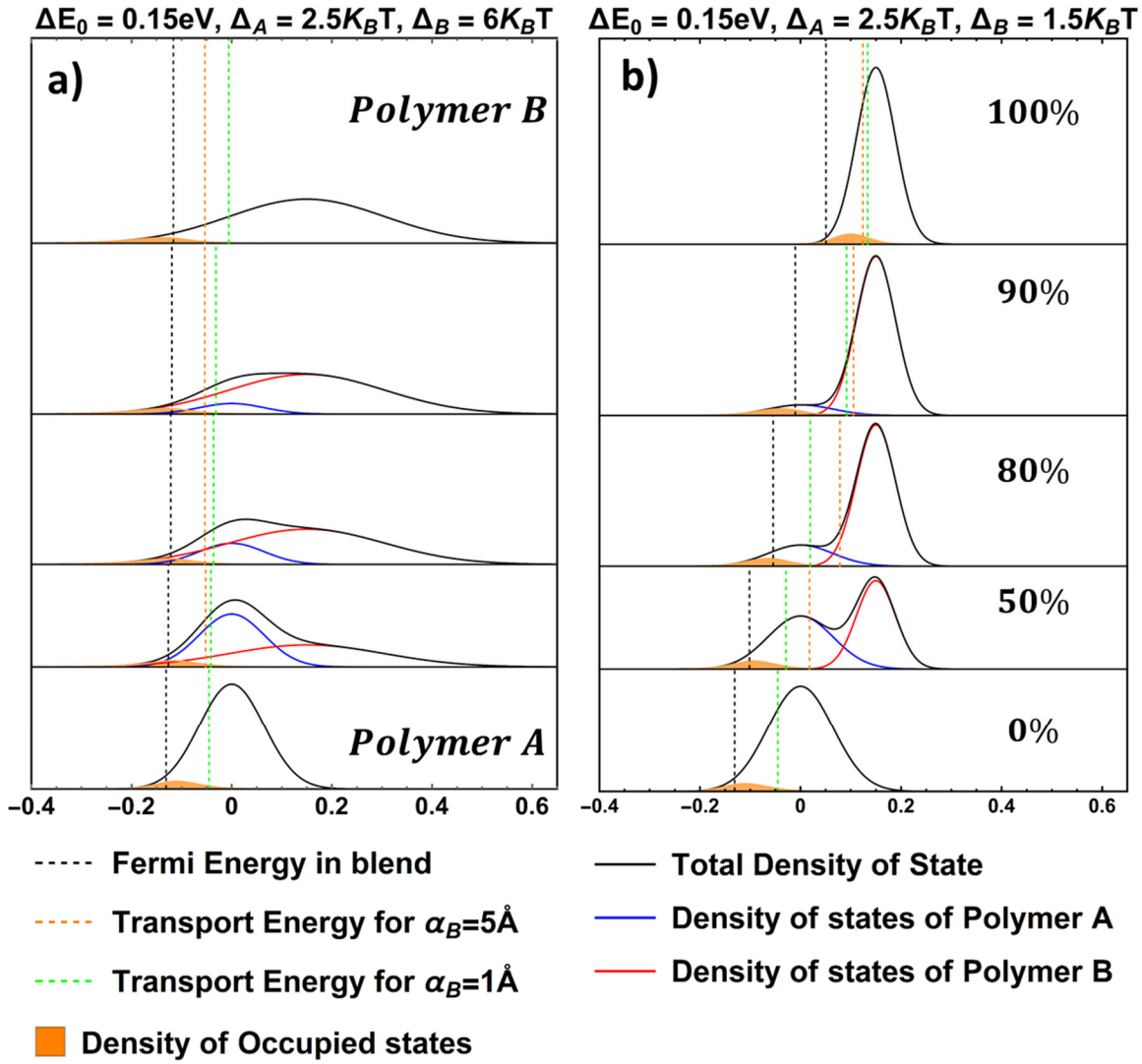


**Figure S4.** Transport energy in polymer blends with varying compositions. In (a) the polymer with its DOS centered at higher energies has a broader DOS ( $\Delta_B = 6 K_B T$ ) than the polymer with its DOS centered at lower energies and in (b) the polymer with the higher energy DOS has a narrower DOS ( $\Delta_B = 1.5 K_B T$ ). In both cases the DOS distributions of the polymers display a 0.15 eV energy offset. To calculate transport energy from equation 9, Polymer A parameters are  $\alpha_A=2\text{\AA}$ ,  $N_{t,A}= 6.1\times 10^{20} \text{ cm}^{-3}$ ,  $\Delta_A=2.5 K_B T$  and  $E_{0,A}=0 \text{ eV}$  and parameters for Polymer B are  $N_{t,B}= 6.1\times 10^{20} \text{ cm}^{-3}$ ,  $\alpha_B=1\text{\AA}$  (Dashed green line) and  $5\text{\AA}$  (Dashed orange line) and  $E_{0,B}=0.15\text{eV}$  ( $\Delta E_0=0.15\text{eV}$ ) and the common parameters are  $v_0=10^{12}\text{s}^{-1}$ ,  $T=300\text{K}$  and  $N_C=3\times 10^{19} \text{ cm}^{-3}$

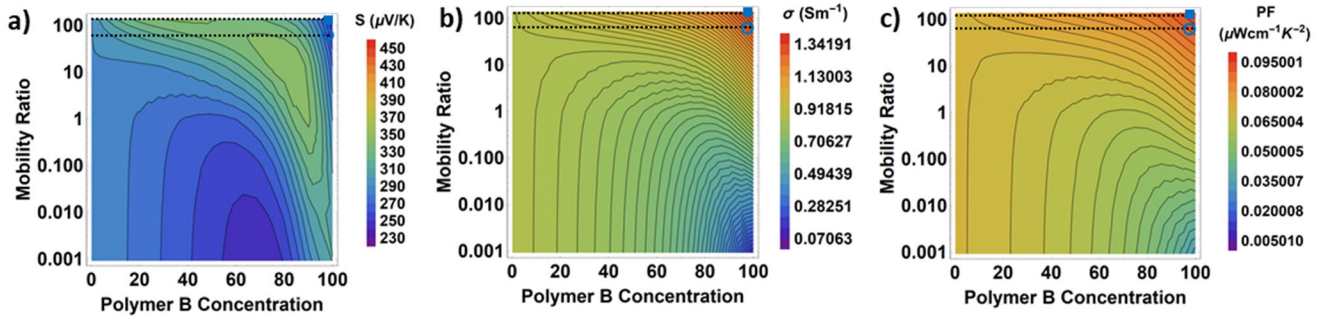


**Figure S5.** (a) Seebeck coefficient, (b) electrical conductivity, and (c) power factor calculated for polymer blends. Polymer A fitting parameters are  $\alpha_A=2\text{\AA}$ ,  $N_{t,A}=6.1\times 10^{20}\text{ cm}^{-3}$ ,  $\Delta_A=2.5\text{ K}_B T$  and  $E_{0,A}=0\text{ eV}$  and fitting parameters for Polymer B are  $N_{t,B}=6.1\times 10^{20}\text{ cm}^{-3}$ ,  $\Delta_B=2.5\text{ K}_B T$  and  $E_{0,B}=0.15\text{ eV}$  ( $\Delta E_0=0.15\text{ eV}$ ) and the common parameters are  $v_0=10^{12}\text{ s}^{-1}$ ,  $T=300\text{ K}$  and  $N_C=3\times 10^{19}\text{ cm}^{-3}$ . Dashed lines correspond to calculations from Fig3. One data line was less than  $10^{-3}$ , so it has been cut from the heat map.

## V. Effective localization length

In case of charge transfer between two localized states with localization length of  $\alpha_A$  and  $\alpha_B$ , we treat the jump rate with the following equation:

$$v \propto \text{Exp}\left[-\frac{r_{ij}}{\alpha_A}\right] \times \text{Exp}\left[-\frac{r_{ij}}{\alpha_B}\right] = \text{Exp}\left[-\frac{2r_{ij}}{\frac{2\alpha_A\alpha_B}{\alpha_A+\alpha_B}}\right] = \text{Exp}\left[-\frac{2r_{ij}}{\alpha_{eff}}\right] \quad (\text{S.9})$$

$\alpha_{eff}$  represents an effective localization length for a jump between two localized states with different localization lengths. Here we assume the localization length of each individual polymer is the same in the blend as in the pure materials. If a charge carrier is located on polymer A initially, the average number of available hopping sites for such charge carrier starting at energy  $E_i$  whose hopping parameter is smaller than  $R$  can be written as:

$$n_A(E_i, R) = \frac{\pi}{6} R^3 C_A \alpha_A^3 \left( \int_{-\infty}^{E_i} g_{u,A}(E_j, E_F) dE_j + \int_{E_i}^{E_i+K_B T R} g_{u,A}(E_j, E_F) \left(1 - \frac{E_j-E_i}{K_B T R}\right)^3 dE_j \right) + \frac{\pi}{6} R^3 C_B \alpha_{eff}^3 \left( \int_{-\infty}^{E_i} g_{u,B}(E_j, E_F) dE_j + \int_{E_i}^{E_i+K_B T R} g_{u,B}(E_j, E_F) \left(1 - \frac{E_j-E_i}{K_B T R}\right)^3 dE_j \right) \quad (\text{S.10})$$

And if the charge carrier is located on polymer B, the same parameter for such charge carrier can be calculated as:

$$n_B(E_i, R) = \frac{\pi}{6} R^3 C_A \alpha_{eff}^3 \left( \int_{-\infty}^{E_i} g_{u,A}(E_j, E_F) dE_j + \int_{E_i}^{E_i+K_B T R} g_{u,A}(E_j, E_F) \left(1 - \frac{E_j-E_i}{K_B T R}\right)^3 dE_j \right) + \frac{\pi}{6} R^3 C_B \alpha_B^3 \left( \int_{-\infty}^{E_i} g_{u,B}(E_j, E_F) dE_j + \int_{E_i}^{E_i+K_B T R} g_{u,B}(E_j, E_F) \left(1 - \frac{E_j-E_i}{K_B T R}\right)^3 dE_j \right) \quad (\text{S.11})$$

We can define the parameter  $n$  in the polymer blend based on the weighted probability of finding the charge carrier in either polymer:

$$n(E_i, R) = C'_A n_A + C'_B n_B \quad (\text{S.12})$$

here  $C'_A$  and  $C'_B$  are the probabilities of finding a charge carrier on polymer A and B, respectively, which can be calculated as below:

$$C'_A = \frac{\int_{-\infty}^{\infty} C_A g_A(E) f_{FD}(E, E_F) dE}{N_C} \quad (\text{S.13})$$

$$C'_B = \frac{\int_{-\infty}^{\infty} C_B g_B(E) f_{FD}(E, E_F) dE}{N_C} = 1 - C'_A \quad (\text{S.14})$$

Further we can calculate TE properties using equations (S6, S8, 7,8 and 9). Figure S6 compares the same calculations as Figure 3 in the manuscript (Fig. S6a,c,e) with calculations where an effective localization length is included (Fig. S6b,d,f). As shown in Fig. S6, including an effective localization length in the calculations has a large impact on TE properties of the blend system, particularly at lower concentrations of polymer B with  $\Delta_B$  equal to  $1.5K_B T$ ,  $2.5K_B T$ . In the model introduced here in the SI, we added a weighted probability to account for whether the charge carriers start from polymer A or polymer B based on their energetics. As shown in Fig. 2, when polymer B has a narrower DOS centered at higher energies than polymer A, the charge carriers will mostly be localized on polymer A rather than polymer B. Therefore, the probability of a charge carrier to jump from polymer B to another site on polymer B is reduced for two reasons. First, the probability of the charge carrier starting on polymer B is low, and second, the unoccupied states on polymer B are at higher energies. This will cause a drop in the Seebeck coefficient and electrical conductivity in Fig. S6 b and d at low concentrations of polymer B. In the case that polymer B has a broader DOS width, the Seebeck coefficient in the blend will not change as much since the probability of finding a charge carrier on polymer A or B will be comparable to the concentrations of polymer A or B in the blend. Accounting for jumps between polymers with this method has a larger impact on electrical conductivity, particularly in the case where  $\alpha_B$  is larger, e.g.,  $5 \text{ \AA}$ . The drop in  $\sigma$  rises from the effective localization length that is smaller than  $\alpha_B$  ( $\alpha_A$  is  $2 \text{ \AA}$ ,  $\alpha_B$  is  $5 \text{ \AA}$  and so  $\alpha_{\text{eff}}$  is  $2.86 \text{ \AA}$ ). The drop in electrical conductivity is significant enough that it reduces the improvement in power factor from 26% to 3%.

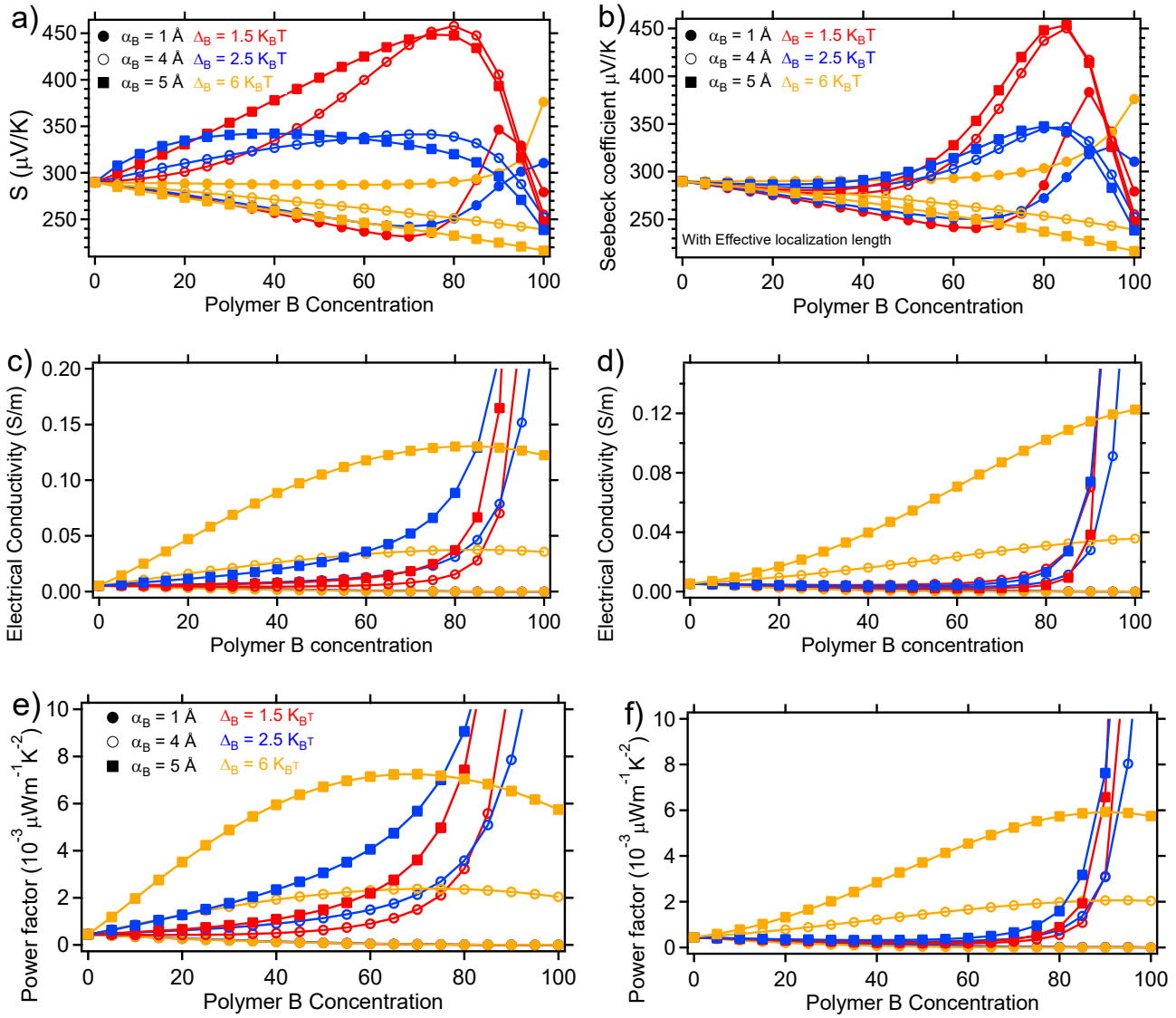


**Figure S6.** (a,b) Seebeck coefficient, (c,d) electrical conductivity and (e,f) power factor of polymer blend systems calculated as described in the paper (a,c,e) and calculated based on an effective  $\alpha$  as described in the SI (b,d,f). Polymer A has fitting parameters of  $\alpha_A=2 \text{ \AA}$ ,  $N_{t,A} = 6.1 \times 10^{20} \text{ cm}^{-3}$ ,  $\Delta_A=2.5 \text{ K}_B T$  and  $E_{0,A}=0 \text{ eV}$  and polymer B has fitting parameters of  $\alpha_B=1, 4$  and  $5 \text{ \AA}$ ,  $N_{t,B} = 6.1 \times 10^{20} \text{ cm}^{-3}$ ,  $\Delta_B=1, 2.5$  and  $6 \text{ K}_B T$  and  $E_{0,B}=0.15 \text{ eV}$  ( $\Delta E_0=0.15 \text{ eV}$ ). Other fit parameters are  $v_0=10^{12} \text{ s}^{-1}$ ,  $T=300 \text{ K}$  and  $N_C=3 \times 10^{19} \text{ cm}^{-3}$ .

By including an effective localization length and accounting for the probability of a charge carrier starting on polymer A or B, the modeled TE properties in polymer blends changes, especially the magnitude of power factor improvement. To determine if we could achieve the same improvement when an effective localization length is accounted for, we probed additional combinations where the two mentioned effects are minimized. To increase the contribution of polymer B to charge carriers conduction, the DOS width of polymer B can be increased or the energetic offset between the two DOS decreased. As is shown in figure S7 a, d and g, by increasing the DOS width of polymer B

from  $6K_B T$  to  $7K_B T$ , similarly large power factor improvements in the blends are achievable again. Similarly, Figure S7 h suggests by reducing the energetic offset from  $0.15$  eV to  $0.1$  eV we can reproduce the power factor improvement. The other effect from this revised model is that the effective localization length is some number between  $\alpha_A$  and  $\alpha_B$ , so by reducing the difference we can reduce the effect of  $\alpha_{eff}$ . As Figure S7 i shows, by reducing the difference between the two localization lengths from  $2\text{\AA}$  to  $1\text{\AA}$ , we can reproduce the power factor improvement. In this section we show that by differentiating between hopping between two different polymers, the parameters where power factor improvements are observed shift slightly. These variations still follow the same trends which are reported in manuscript with one additional comment, the localization length between two polymers should not be overly different.

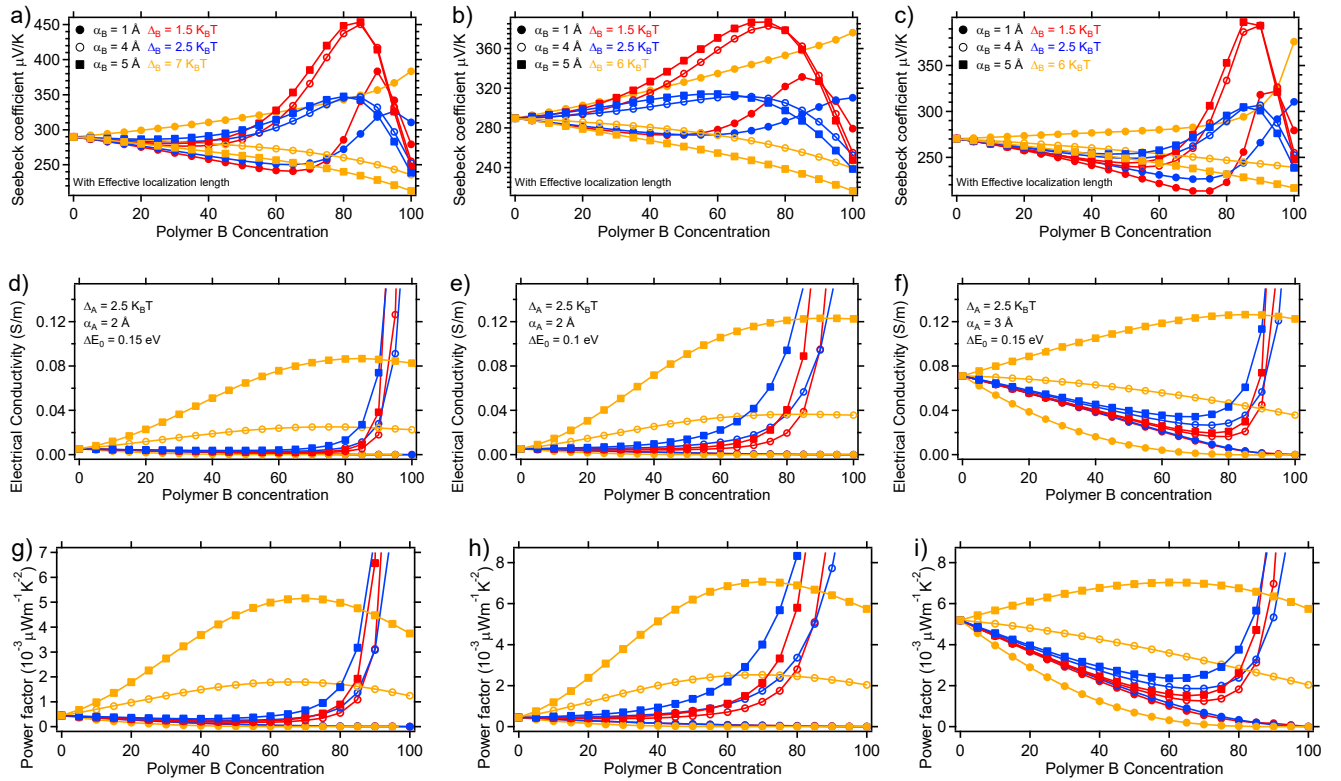


**Figure S7.** (a, b, c) Seebeck coefficient, (d, e, f) electrical conductivity and (g, h, i) power factor of polymer blend systems. Each column presents slight variations in parameters where power factor improvements in the blends are expected. In figures a, b, d, e, g and h polymer A has fitting parameters of  $\alpha_A=2\text{\AA}$ ,  $N_{t,A}=6.1\times 10^{20}\text{ cm}^{-3}$ ,  $\Delta_A=2.5 K_B T$  and  $E_{0,A}=0$  eV and figures c, f and i all parameters for polymer A are same except for localization length which the value is  $\alpha_A=3\text{\AA}$ . Polymer B has fit parameters of  $\alpha_B=1,4$  and  $5\text{\AA}$ ,  $N_{t,B}=6.1\times 10^{20}\text{ cm}^{-3}$ ,  $\Delta_B=1, 2.5$  and  $6 K_B T$  ( $6 K_B T$  for figure a, d and g) and  $E_{0,B}=0.15$  eV ( $\Delta E_0=0.15$  eV, for figure b, e and h the value is  $\Delta E_0=0.1$  eV). Other fit parameters are  $v_0=10^{12}\text{ s}^{-1}$ ,  $T=300$  K and  $N_C=3\times 10^{19}\text{ cm}^{-3}$ .

The theoretical fitting to the experimental data from the manuscript and the revised version from this section where  $\alpha_{\text{eff}}$  is applied are shown in Figure S8 to show how accounting for jumps between polymer A and B alters the results. Figure 8 shows that using an effective localization length has a minimum effect on PDPP-4T:RRa-P3HT and PDPP-4T:PDPP-T-TT-T blend systems. The effect is minimized in PDPP-4T:PDPP-T-TT-T blends because PDPP-T-TT-T has a similar DOS width with a small energetic offset compared to PDPP-4T. The new theoretical approach doesn't change the trend in PDPP-4T:RRa-P3HT blend because RRa-P3HT already has very small localization length, so the effect on the power factor is negligible. As we can see in Figure S8 a and b, using the same parameters as Table 1 with the new theoretical approach applied the calculated data deviates more from the experimental data and does not show as much improvement in the power factor for the reasons explained previously. However, as shown in figure S9, reducing the energetic offset from 0.15 to 0.1eV between PDPP-4T and RRa-P3HT does fit the experimental data well and shows a similar improvement in power factor as the data reported in the manuscript.

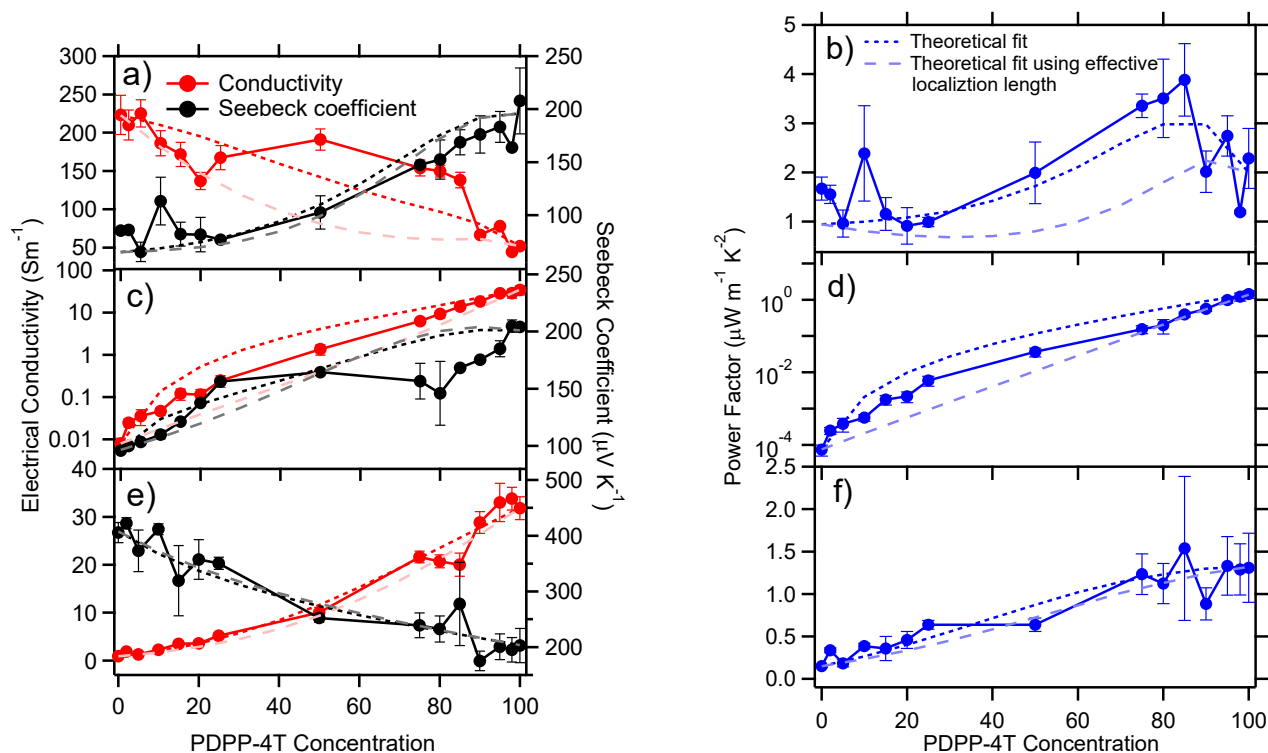


**Figure S8.** (a,c,e) Seebeck coefficient and electrical conductivity and (b,d,f) power factor as a function of PDPP-4T concentration in the polymer blend. The blends are PDPP-4T:RR-P3HT (a,b) and PDPP-4T:RRa:P3HT (c,d) and PDPP-4T:PDPP-T-TT-T (e,f). Darker dashed lines with shorter dashes are the fits to the model as calculated with equations 7 and 8 and lighter dashed lines with longer dashes are the fits to the model accounting for effective localization length. The fitting parameters can be found in Table 1.

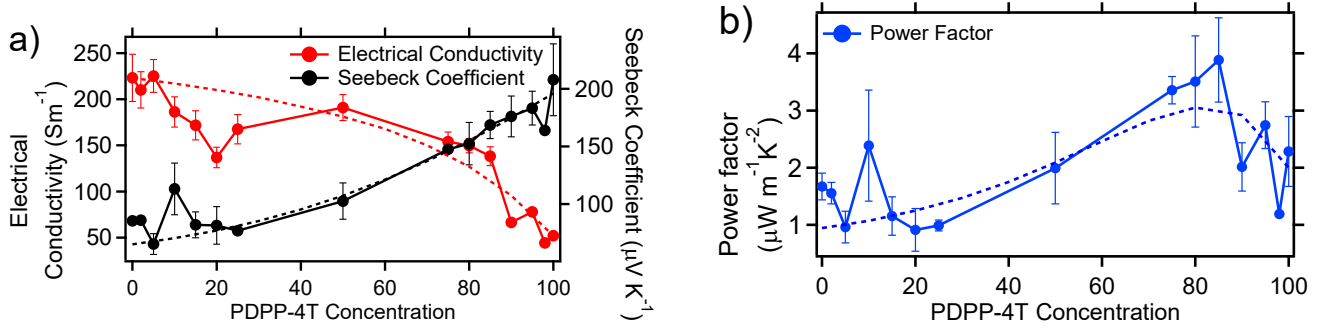


**Figure S9.** (a) Seebeck coefficient and electrical conductivity and (b) power factor as a function of PDPP-4T concentration in the PDPP-4T:RR-P3HT blend when  $E_0$  is reduced from 0.15 eV (see Figure S8) to 0.10 eV. Dashed lines are the fits to the model as calculated with accounting for effective localization length with the fitting parameters listed in Table 1, except here  $E_0=0.1$  eV.

*Calculation:* calculations were done using Mathematica<sup>9</sup>

## VI. Fitting parameters in polymer blends

The number of electronic states per unit volume were calculated based on the density and molecular weight of the polymer and dopant using equations S.15 and S.16.

$$N_d = \left( \gamma^{-1} \frac{MW_p}{\rho_p} + \frac{MW_d}{\rho_d} \right)^{-1} N_A \quad \text{S.15}$$

$$N_p = \left( \frac{MW_p}{\rho_p} + \gamma \frac{MW_d}{\rho_d} \right)^{-1} N_A x \quad \text{S.16}$$

Where  $N_d$  is the number of dopant molecules per unit volume,  $N_p$  the maximum number of aromatic rings in the polymer backbone per unit volume of polymer,  $N_A$  is Avogadro's number,  $MW_p$  is the molecular weight of a repeat unit in the polymer,  $MW_d$  the molecular weight of dopant,  $\rho_p$  the density of polymer,  $\rho_d$  the density of dopant,  $\gamma$  the ratio of dopant molecules to polymer repeat units and  $x$  is equal to the number of aromatic rings in the polymer repeat unit. The total number of states is always smaller than the maximum number of aromatic rings contributed by the polymer ( $N_t \leq N_p$ ) and the number of charge carriers are always smaller than the number of dopants ( $N_c \leq N_d$ ). Table S1 shows these parameters for the four polymers we used in this study.

**Table S1.** The molecular weight of a polymer repeat unit and the density of polymers (estimated) and dopant.  $\gamma$  is extracted from solution preparation and concentration of dopant and maximum number of states are calculated using equation S15 and S16.

material	$MW$ (g/mol)	$\rho$ (g/cm <sup>3</sup> )	$\gamma\%$	$x$	$N_d$ (10 <sup>19</sup> cm <sup>-3</sup> )	$N_p$ (10 <sup>20</sup> cm <sup>-3</sup> )
PDPP-4T	1024.6	1.2	32	6	20.2	37
PDPP-T-TT-T	1110.71	1.2	35	6	20.3	35
RR-P3HT	166.28	1.2	5.3	1	20.3	38
RRa-P3HT	166.28	1.2	5.3	1	20.3	38
Mo(tfd) <sub>3</sub>	774.43	2.27				

To calculate the number of charge carriers in the polymer blends, we used equation S.17:

$$N_{C,Blend} = C_A N_{C,A} + C_B N_{C,B} \quad \text{S.17}$$

$N_{C,Blend}$  is the number of charge carriers in the blend,  $C_A$  and  $C_B$  are the concentrations of polymer A and B and  $N_{C,A}$  and  $N_{C,B}$  are the number of charge carriers for pure polymer A and pure polymer B.

To estimate the attempt to jump frequency in the blend system we have used a similar equation:

$$\vartheta_{0,Blend} = C_A \vartheta_{0,A} + C_B \vartheta_{0,B} \quad \text{S.18}$$

Where

$$\vartheta_{0,A} = \frac{\sigma_{Exp,A}}{\sigma_{Theory,A}}, \quad \vartheta_{0,B} = \frac{\sigma_{Exp,B}}{\sigma_{Theory,B}} \quad \text{S.19,20}$$

$\sigma_{Exp}$  is the experimentally measured electrical conductivity and  $\sigma_{Theory}$  is the theoretical electrical conductivity assuming  $\vartheta_0$  in equation 7 is equal to 10<sup>12</sup>s<sup>-1</sup>.

## VII. PDS

Photothermal deflection spectroscopy (PDS) is a highly sensitive technique to measure optical absorption in thin films.<sup>10</sup> Chopped, monochromatic light from a 300 W Xe light source was coupled into a monochromator with  $\pm 4$  nm wavelength resolution and focused onto the sample surface to cause a periodic temperature change in the focal spot region. The sample was immersed in a fluid (Fluorinert FC72) with a high thermo-optic coefficient and the periodic temperature change of the sample caused a corresponding temperature and index of refraction change in the fluid. A CW probe beam from a HeNe laser passed through the fluid and across the sample surface, deflecting along its path as it encounters variations in index of refraction. The probe beam position was monitored by a quadrant-cell photodiode that was fed into a lock-in amplifier to measure the periodic deflection. Spectral measurements were achieved by varying the excitation wavelength over the range of interest. The schematic figure and

picture of the setup is shown in figure S10. Long-pass optical filters were installed at the input and output of the monochromator to reduce undesired wavelengths at the sample surface. The excitation beam was chopped at 9 Hz for these measurements; further details of the PDS apparatus used in this study can be found elsewhere.<sup>11</sup>

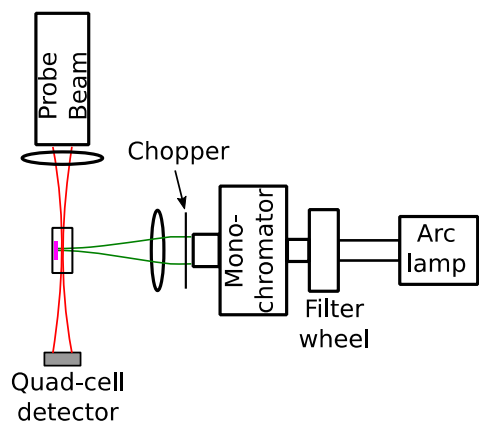


**Figure S10.** Schematic of the PDS setup.

PDS measurements done on undoped polymers are in good agreement with the optical absorbance as shown in Fig S12.b. The Urbach energies were extracted using equation S.21 to fit the sub-gap region of the PDS spectrum.<sup>12</sup>

$$Abs = a_0 e^{\frac{E-E_g}{E_u}} \quad (E < E_g) \quad (S.21)$$

Where  $Abs$  is absorbance,  $a_0$  is a constant,  $E$  is the energy of the absorbed photon,  $E_g$  is the band gap energy and  $E_u$  is Urbach energy. The Urbach energy of each polymer is shown in Figure S12a.

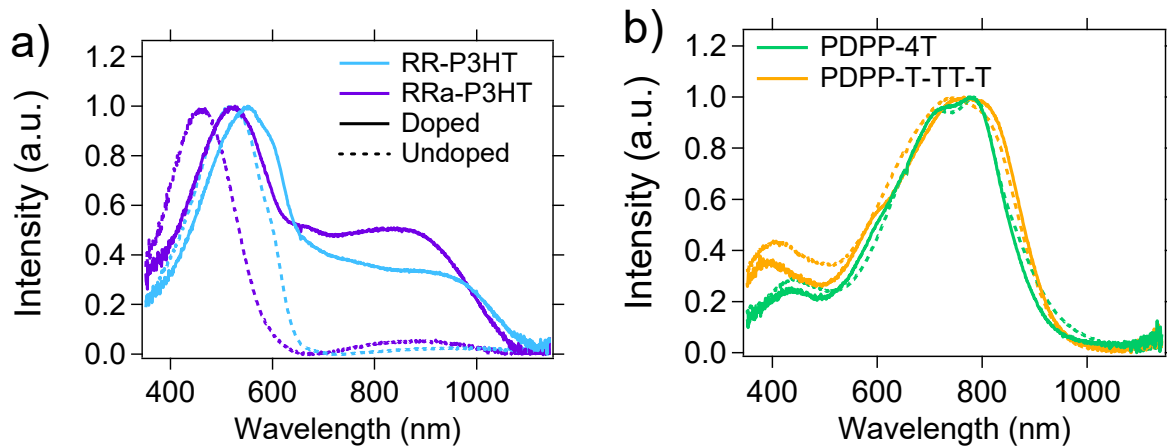


**Figure S11.** UV-Vis spectrum of doped and undoped (a) RR-P3HT and RRa-P3HT and (b) PDPP-4T and PDPP-T-TT-T. Polarons band can be seen for RR-P3HT and RRa-P3HT.

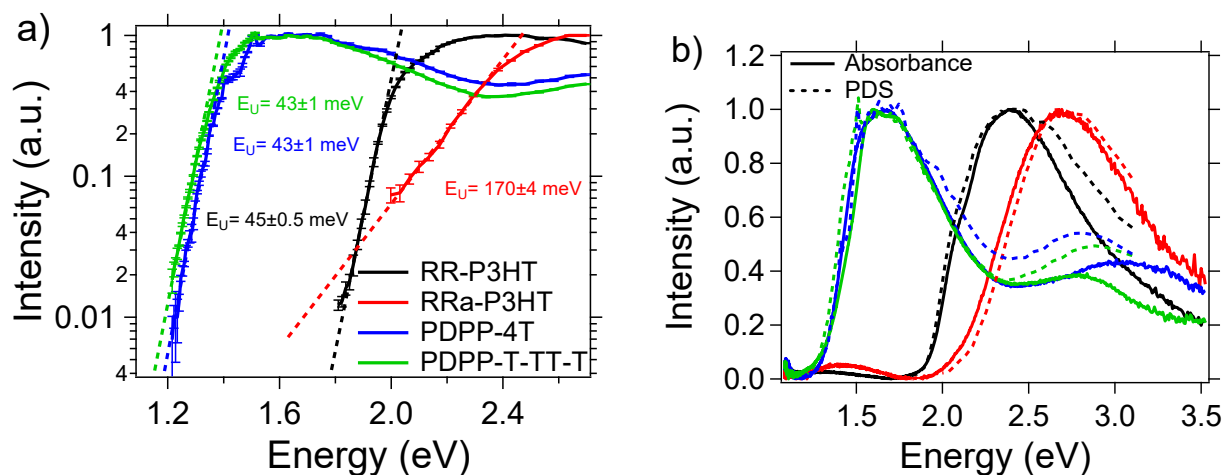


**Figure S12.** (a) PDS spectrum of all undoped polymers on a logarithmic scale and their Urbach energies extracted from equation S21. (b) PDS (dashed) and UV-Vis (solid line) spectrum of undoped polymers which shows the agreement between two measurements. The dip in absorbance at the absorbance edge is due to polymer photoluminescence.

## VIII. AFM

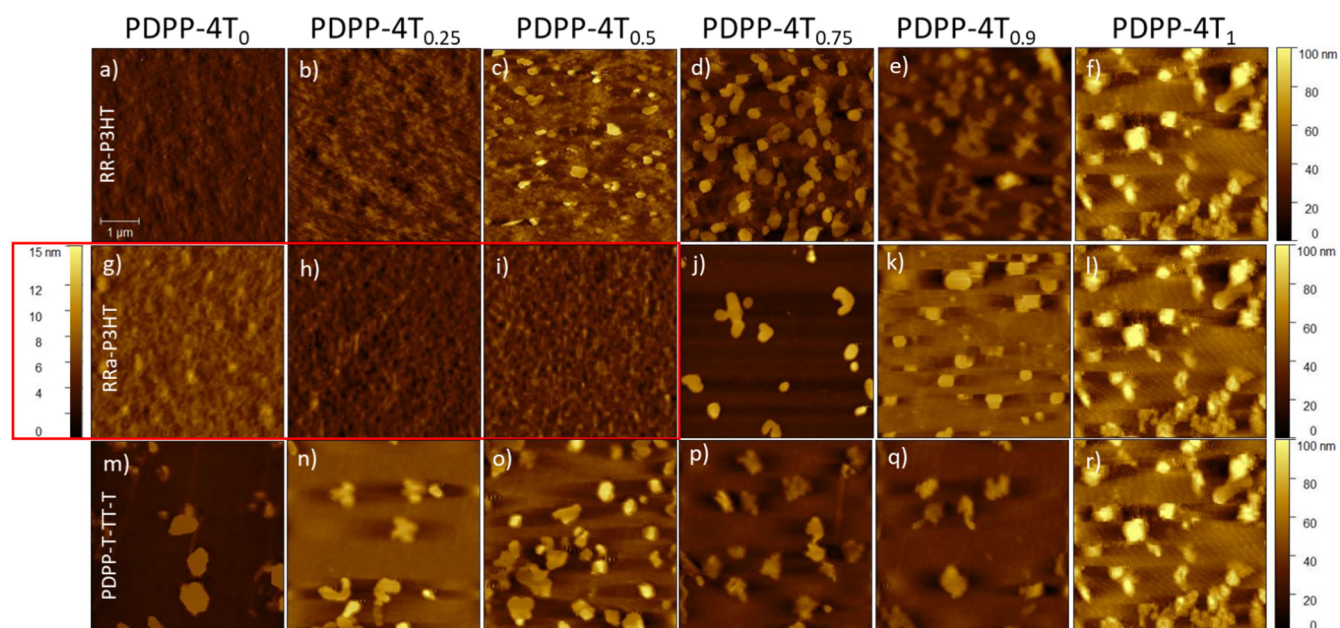


**Figure S13.** AFM on polymer blend system of RR-P3HT:PDPP:4T (a-f), RRa-P3HT:PDPP-4T (g-l) and PDPP-T-TT-T:PDPP-4T (m-r). Concentration of PDPP-4T in blend system is shown at top each column. Figures g, h and i have different scale which are separated by the red box.

## Reference:

- 1 A. Davison, R. H. Holm, R. E. Benson and W. Mahler, in *Inorganic Syntheses*, 2007, vol. X, pp. 8–26.
- 2 Y. Zhao, X. Zhao, Y. Zang, C. A. Di, Y. Diao and J. Mei, *Macromolecules*, 2015, **48**, 2048–2053.
- 3 B. C. Schroeder, T. Kurosawa, T. Fu, Y.-C. Chiu, J. Mun, G.-J. N. Wang, X. Gu, L. Shaw, J. W. E. Kneller, T. Kreouzis, M. F. Toney and Z. Bao, *Adv. Funct. Mater.*, 2017, **27**, 1701973.
- 4 Z. Liang, M. J. Boland, K. Butrouna, D. R. Strachan and K. R. Graham, *J. Mater. Chem. A*, 2017, **5**, 15891–15900.
- 5 A. M. Boehm, J. Wieser, K. Butrouna and K. R. Graham, *Org. Electron.*, 2017, **41**, 9–16.
- 6 I. V. Arkhipov, P. Heremans, E. V. Emelianova, G. J. Adriaenssens and H. Bässler, *J. Phys. Condens. Matter*, 2002, **14**, 9899–9911.
- 7 I. I. Fishchuk, V. I. Arkhipov, A. Kadashchuk, P. Heremans and H. Bässler, *Phys. Rev. B - Condens. Matter Mater. Phys.*, 2007, **76**, 1–12.
- 8 D. Mendels and N. Tessler, *J. Phys. Chem. Lett.*, 2014, **5**, 3247–3253.
- 9 I. Wolfram Research, 2017.
- 10 W. B. Jackson, N. M. Amer, A. C. Boccara and D. Fournier, *Appl. Opt.*, 1981, **20**, 1333.
- 11 B. Couch, A. Meyer, B. Heller and S. L. Johnson, *Methods Appl. Fluoresc.*, 2018, **7**, 015004.
- 12 D. Venkateshvaran, M. Nikolka, A. Sadhanala, V. Lemaire, M. Zelazny, M. Kepa, M. Hurhangee, A. J. Kronemeijer, V. Pecunia, I. Nasrallah, I. Romanov, K. Broch, I. McCulloch, D. Emin, Y. Olivier, J. Cornil, D. Beljonne and H. Sirringhaus, *Nature*, 2014, **515**, 384–388.